

Local Thermal Non-Equilibrium Effect in Solid Oxide Fuel Cells with Various Fuels

Keqing Zheng, Qiong Sun, Meng Ni*

Building Energy Research Group, Department of Building and Real Estate
The Hong Kong Polytechnic University, Hung Hom, Kowloon, Hong Kong, China

Abstract:

Local thermal equilibrium (LTE) is a common assumption used in thermal modeling of solid oxide fuel cells (SOFCs). However, its validity has not been well confirmed. To examine the validity of the LTE assumption, a thermal model is developed to evaluate the local thermal non-equilibrium (LTNE) effect of SOFC electrodes with various fuels, considering methane internal reforming and ammonia thermal cracking in anode. Although the LTNE effect for ammonia fed SOFC is more pronounced than that for hydrogen fed SOFC, the LTE assumption can be safely adopted for SOFC modeling for a wide range of operating/structural parameters and for various fuels, such as hydrogen, ammonia, and methane.

Keywords:

Fuel cell; Modeling; Heat transfer; Thermodynamics; Steam Reforming.

* Corresponding author. Tel: (852) 2766 4152; Fax: (852) 2764 5131;
Email: meng.ni@polyu.edu.hk (Meng Ni)

1. Introduction

Solid oxide fuel cell (SOFC), a promising power generation device with high efficiency, has attracted much attention in recent years. Mathematical modeling is a valuable tool to investigate the complicated physical-chemical processes in SOFCs as well as to optimize the operating/structural parameters of SOFC stacks [1]. In almost all thermal modeling studies of SOFCs, it is a common practice to assume local thermal equilibrium (LTE), that means the temperature of the gas species is locally the same with the temperature of the solid structure [2]. The LTE assumption considerably simplifies the computation, as only one energy equation is required for the whole computational domain. However, its validity has not been well confirmed yet.

An early study on the local thermal non-equilibrium (LTNE) effect in proton exchange membrane fuel cell (PEMFC) was conducted by Hwang and Chen [2]. A dimensionless LTNE criterion was proposed and the significance of LTNE effect was examined under typical structural parameters and operation conditions [2]. Subsequently, Damm and Fedorov questioned the LTE assumption for SOFC electrodes [3]: first, gas phase is mainly transported by diffusion in porous electrodes which may lead to a low Reynolds number and thus a low heat transfer rate; second, heat generation/consumption takes place where electrochemical/chemical reactions occur, especially when hydrocarbon fuels or ammonia are used. To address this issue, Damm and Fedorov [3] investigated the local heat transfer in the porous electrode of hydrogen fueled SOFC with the magnitude analysis method. Their study provides an excellent framework to examine the temperature difference between the gas phase and the solid structure in an SOFC. However, only H₂ fuel is considered and their study only

examines some typical working conditions. Since fuel flexibility is a major attraction for SOFCs and the internal reforming of hydrocarbon fuels or thermal cracking of ammonia can significantly influence the thermal field of the SOFCs, it is necessary and important to examine the validity of LTE in SOFCs running on alternative fuels. However, from the literature, no such study has been performed yet. In addition, Damm and Fedorov's study [3] might underestimate the temperature difference because they overestimate the heat generation area by using the whole pore surface area in their analysis. It should be mentioned that in an SOFC, electrochemical reaction occurs only at the triple-phase boundary (TPB) region. Thus it is appropriate to consider the whole particle surface as the heat transfer area if the heat conductivity of the solid is very high, while this treatment may not be valid if the heat conductivity of the solid is not high enough.

Due to the above reasons, a more comprehensive study is performed in the present work to evaluate the LTNE effect in SOFC porous electrodes by examining the temperature difference between the gas and the solid. Different from ref. [3] that only consider hydrogen fuel for SOFCs, alternative fuels are considered in the present study. The reaction heats for chemical reactions are included in this study, such as methane steam reforming (MSRR) and ammonia thermal cracking reaction (ACR). The upper limit of temperature difference between the gas phase and the solid phase (ΔT_{sf}) is used as an indicator for the LTNE effect [3]. Also different from Damm and Fedorov's work [3], the TPB zone, instead of the whole particle surface, is used as the heat transfer area for ΔT_{sf} estimation. Since half-reactions occurring in anode and cathode are different, heat generation or consumption from half-reactions are calculated separately in each porous electrode. All overpotential losses are

considered. The study considers typical SOFC materials – yttria-stabilized zirconia (YSZ) electrolyte, Ni-YSZ anode, and lanthanum strontium manganite (LSM)-YSZ cathode. However, other SOFC materials can be easily studied by simply modify the material parameters.

2. Thermal analysis

In SOFC porous electrodes, electrochemical reactions accompanied with large amount of heat generation/consumption occur in the TPB region (as shown in Fig.1, intersection zone of gas phase, electronic conducting phase, and ionic conducting phase). Thermal energy dissipation from the surface of the solid structure occurs by three ways simultaneously: (1) conduction to other parts of solid particles; (2) convection from solid phases to gas phases; and (3) radiation to other electrode particles. Based on Damm's method, the temperature difference between solid and gas phase (ΔT_{sf}) is used as an indicator for the LTNE effect and only convection heat transfer is considered [3]. Since conduction and radiation heat transfer provide additional way for heat dissipation which tends to reduce the temperature difference, it is reasonable to neglect the conduction and radiation to focus on the upper value of ΔT_{sf} .

According to Hwang and Chen [2], the gas-solid temperature difference ΔT_{sf} can be obtained as:

$$\Delta T_{sf} = T_s - T_f = \frac{Q}{h_{sf} a_s} \quad (1)$$

where Q is the volumetric heat generation/consumption coupled with electrochemical/chemical reactions (Wm^{-3}); h_{sf} is the heat transfer coefficient between gas

and solid phases ($\text{Wm}^{-2}\text{K}^{-1}$), a_s is the specific (volumetric) heat transfer area (m^2m^{-3}).

2.1 Convection heat transfer coefficient

In the porous electrodes of SOFC, gas transport occurs mainly by means of diffusion. It is reported that the gas phase velocity and Reynolds number (R_e) in porous electrode of PEMFC are 0.239ms^{-1} and 0.004 when the current density and porosity are 10^4Am^{-2} and $0.3\mu\text{m}$, respectively [2]. Consequently, relationship developed by Kuwahara [4] is adopted in the present work to calculate h_{sf} (valid for a broad range of Reynolds number, Prandtl number, particle size and porosity):

$$\frac{h_{sf}d}{k_f} = \left(1 + \frac{4(1-\theta_p)}{\theta_p} \right) + 0.5(1-\theta_p)^{0.5} \text{Re Pr}^{\frac{1}{3}} \quad (2)$$

where, θ_p is porosity of electrode; k_f is thermal conductivity of fluid, $\text{Wm}^{-1}\text{K}^{-1}$; d is solid particle diameter, μm . Considering R_e for gas phase in porous electrode is far less than unit, and $Pr=0.7\sim 0.8$ (for common gases), the second item on the right side of Eq. (2) can be safely neglected. As a result, h_{sf} can be determined as,

$$h_{sf} = \left(1 + \frac{4(1-\theta_p)}{\theta_p} \right) \frac{k_f}{d} \quad (3)$$

2.2 heat transfer area

In the SOFC electrodes, electrochemical reactions occur only at the TPB region. Thus, in the present study, the TPB zone is considered as the sites for heat generation/consumption from electrochemical reaction and overpotential losses to find the upper limit of ΔT_{sf} . The formula proposed by Gokhale [5] has been commonly used for calculating the TPB length (L_{TPB}) and thus is used in the present study (valid for any isotropic uniform-random three phase microstructure):

$$L_{TPB} = \frac{\pi}{4} F_1(\alpha) F_2(\theta_p) F_3(K) F_4(CV, \gamma) \frac{1}{D_L D_Y} \quad (4)$$

where: $F_1(\alpha)$ reflects the effect of composition ratio in the electrodes, which varies no more than 10% for $0.5 \leq \alpha \leq 2.5$ [5]. Here, $F_1(\alpha)$ equals to 0.225. $F_2(\theta_p)$ represents the effect of porosity on L_{TPB} . $F_3(K)$ reflects the effect of particle shape on L_{TPB} . It equals to 36 for spherical particles. $F_4(CV, \gamma)$ reflects the effect of size distribution on L_{TPB} . It equals to 1 for mono-size particles.

For mono-size spherical particles, the TPB length can be calculated as,

$$L_{TPB} = 6.36 \frac{\theta_p (\ln \theta_p)^2}{d^2} \quad (5)$$

Furthermore,

$$a_s = w \cdot L_{TPB} \quad (6)$$

where, w refers to effective width of TPB region, nm.

2.3 Heat generation or consumption

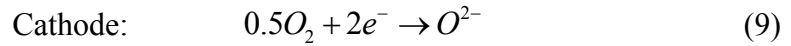
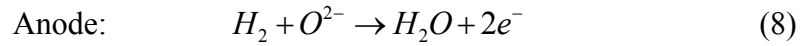
In SOFC, heat sources (and their locations) can be summarized as follows [6]:

- a. half-reaction (TPB region in electrodes)
- b. Concentration loss(electrodes)
- c. Activation loss (TPB region in anode)
- d. Ohmic loss (electrodes and electrolyte)
- e. Methane reforming reaction (anode)
- f. Ammonia thermal cracking reaction (anode)
- g. Water gas shifting reaction (gas channel and anode)

2.3.1. Half-reactions in single electrodes

In ref. [3], the overall electrochemical reaction heat is applied to the anode. However, since the hydrogen oxidation and oxygen reduction reaction occur separately in the anode and the cathode, the corresponding reaction heats for anode and cathode should be calculated separately as well.

The primary hydrogen oxidation reaction in SOFC electrodes can be divided into two half-reactions in anode and cathode respectively,



Reversible heat generation due to electrochemical reaction (Q_{rev}) can be obtained by:

$$Q_{rev} = -T\Delta S \frac{i}{nFL} \quad (10)$$

Where entropy change of half-reaction in single electrode can be calculated based on Seebeck coefficient which is used in the electrochemical community and defined as $\Delta E/\Delta T$ [7]:

$$\frac{\Delta E}{\Delta T} = \frac{\Delta S}{nF} \quad (11)$$

It should be noticed that Seebeck coefficient is usually experimentally determined. Here a value of -0.463mVK^{-1} is used according to Ratkje and Tomii's research on SOFCs at typical operating conditions, which are applicable to the present study [8]. Thus the entropy change of oxygen reduction reaction in cathode can be obtained:

$$\Delta S^C (T_{1273K}, P_{O_2, 1atm}) = -89.27 \text{ Jmol}^{-1} \text{ K}^{-1} \quad (12)$$

Based on this, entropy change of oxygen reduction half-reaction in cathode at any

temperature and oxygen partial pressure can be calculated as follows [7]:

$$\Delta S^C(T, P_{O_2}) = \Delta S^C(T_{1273K}, P_{O_2, 1atm}) + R \ln \left(\frac{P_{O_2}}{P_{O_2, 1atm}} \right) \quad (13)$$

Therefore, entropy change of hydrogen oxidation half-reaction in anode can be obtained using Eq. (14) when total entropy change ΔS of H₂-O₂ reaction is known (Eq. (15)):

$$\Delta S^a = \Delta S - \Delta S^C \quad (14)$$

$$\Delta S(T, P_i) = \Delta S(T) + R \ln \left(\frac{P_{H_2} (P_{O_2})^{0.5}}{P_{H_2O}} \right) \quad (15)$$

2.3.2. Overpotential losses

Irreversible heat generation caused by electrochemical losses is more complicated to deal with because of different heat generation locations as shown in Section 2.3. Thus, in this paper, maximum heat generation amount due to electrochemical losses (Q_{loss}) is analyzed together (Eq. (16)) while TPB region is considered as heat generation site. This treatment is reasonable since activation loss is usually dominated over other losses, especially for SOFCs with thin film electrolyte.

$$Q_{loss} = (-\Delta H + T\Delta S) \frac{i}{nFL} \quad (16)$$

2.3.3. Direct internal reforming reaction and ammonia thermal cracking reaction

Different from previous studies focusing on H₂-fueled SOFCs, methane steam reforming reaction (MSRR) and ammonia thermal cracking reaction (ACR) are considered in the present study. Both MSRR and ACR are endothermic, and corresponding heat consumption can be calculated as follows:

$$Q_{MSRR} = -r_{MSRR} \cdot \Delta H_{MSRR} \quad (17)$$

$$Q_{ACR} = -r_{ACR} \cdot \Delta H_{ACR} \quad (18)$$

where, r_{MSRR} and r_{ACR} are reaction rates of MSRR and ACR respectively ($\text{molm}^{-3}\text{s}^{-1}$), which are strongly related to operation temperature and can be approximated by[9, 10],

$$r_{MSRR} = 2395 \exp\left(\frac{-231266}{RT}\right) P_{CH_4} P_{H_2O} \quad (19)$$

$$r_{ACR} = 4 \times 10^{10} \exp\left(\frac{-196200}{RT}\right) P_{NH_3} \quad (20)$$

In practice, a steam-carbon ratio of 2.0 is usually required for CH_4 fed SOFC in order to avoid carbon deposition [11]. Thus, the value of P_{CH_4} and P_{H_2O} are 0.33×10^5 Pa and 0.67×10^5 Pa for r_{MSRR} calculation here. P_{NH_3} is partial pressure of NH_3 , and it equals to 10^5 Pa.

ΔH_{MSRR} and ΔH_{ACR} refer to enthalpy change of MSRR and ACR, Jmol^{-1} . In this study, they can be estimated as[12]:

$$\Delta H_{MSRR} = 206205.5 + 19.5175T \quad (21)$$

$$\Delta H_{ACR} = 40265.095 + 24.23214T - 0.00946T^2 \quad (22)$$

It should be mentioned that in CH_4 fed SOFC, water gas shift reaction (WGSR) can also occur. The WGSR is slightly exothermic and tends to increase the SOFC temperature. However, since the rate of WGSR is usually much smaller than that of MSRR [12], its effect is neglected in the present study for simplicity. According to the authors' best knowledge, no experiments have been conducted to explore the temperature field of the SOFC porous electrodes. Thus it's difficult to validate the present model at this stage. However, the results from this study can be readily compared with relevant experimental data once they are available.

3. Results and analysis

Based on analysis above and Eq.s (1), (3) and (5), the temperature difference between the solid and the gas phase (ΔT_{sf}) can be evaluated by Eqs. (23) and (24). (It should be noted that Q refers to different values in various analysis processes, as listed in Fig.2-Fig.7). In this section, parametric analysis is performed to examine the ΔT_{sf} under various operating conditions and various structural parameters. The effect of MSRR and ACR on LTNE effect is also studied and discussed.

$$\Delta T_{sf} = \frac{Qd^3}{6.36wk_f f(\theta_p)} \quad (23)$$

$$f(\theta_p) = \theta_p (\ln \theta_p)^2 \left(1 + \frac{4(1-\theta_p)}{\theta_p} \right) \quad (24)$$

3.1 Effects of operating temperature and particle size

For H₂ fed SOFCs, heat generation in SOFC mainly consists of two parts: heat from electrochemical reaction (Q_{rev}) and heat from irreversible overpotential losses (Q_{loss}). Based on Eq. (21) and Eq. (22), ΔT_{sf} in anode and cathode at different operation temperatures (800~1200K) is given in Fig.2. It is found that the value of ΔT_{sf} for anode is negative when only Q_{rev} is included while it is positive for cathode. This means that the half reactions in the anode and cathode are endothermic and exothermic, respectively. When both Q_{loss} and Q_{rev} are considered, the value of ΔT_{sf} for anode is changed to positive. This indicates that the heat generation from overpotential losses exceeds the heat consumption by half reaction at the anode. In addition, the anode ΔT_{sf} is found to decrease with increasing temperature. In general, the calculated ΔT_{sf} is on the order of 10^{-3} K, which is about 10 times larger than that obtained from Damm and Fedorov's criteria under the same structural parameters and operation condition [3]. This might be because the heat transfer surface used here (TPB

region) is far less than the whole pore surface area used in Damm and Fedorov's work.

It should be noted that when the particle diameter is increased from 0.3 μm to 0.4 μm , the value of ΔT_{sf} increased significantly (2.37 times), as shown in Fig. 2. The strong dependence of ΔT_{sf} on particle size can be seen from Eq. (23), as larger particles considerably decrease the heat transfer area.

3.2 Effect of porosity θ_p

In order to allow effective gas diffusion and electron/ion conduction, the porosity of SOFC electrodes can't be too low or too high. In the present study, ΔT_{sf} is calculated with varying θ_p from 0.2 to 0.6. It is found that the ΔT_{sf} increases with increase porosity, especially when the porosity is larger than 0.5 (Fig. 3). This is because high porosity leads to small heat transfer area as well as heat transfer coefficient (see Eqs. (3), (5) and (6)). From our analysis, a new relationship of $f(\theta_p)$ is derived from fitting with the simulation results:

$$f(\theta_p) = 34.62 \exp(-6.78\theta_p) \quad (25)$$

For θ_p in range of 0.2~0.6, $f(\theta_p)$ using eq. (25) leads to less than 10% deviation from its value using eq. (20), as well as ΔT_{sf} . Thus, eqs. (23) and (25) provide a more clear relationship between ΔT_{sf} and θ_p and can be used for ΔT_{sf} prediction.

3.3 Effect of TPB width w and reaction depth L

The exact spatial extension of TPB, which is termed as "TPB width", remains to be determined [13]. F.H. van Heuveln[14] reported that the TPB width (W_{TPB}) was no more than 50 nm at YSZ/LSM interfaces at 1218 K[15], while another research claimed that the value

was less than 22 nm[16]. Therefore, in this work, 20 nm is used as typical TPB zone width. However, variations of ΔT_{sf} are calculated with different w (5~50nm), as shown in Fig.4. The result shows that as w increases, large heat transfer surface is created and small ΔT_{sf} is obtained. The reaction depth (L) in the electrode is another important parameter in SOFC which is affected by many operation factors. 10 μ m was used as reaction depth in Damm's research[3] while 2.4 μ m and 6.2 μ m was reported in cathode and anode respectively in another SOFC modeling [17]. The reaction depth in the electrode mainly depends on the ionic conductivity of the electrode and the operating temperature [18]. It's expected that at a lower temperature (i.e. 673K), the reaction depth could be small due to the slow ion conduction from the electrolyte to the electrode. In the present study, ΔT_{sf} with different reaction depths are calculated. It is found that as L decreases, the ΔT_{sf} (Fig. 5) increases due to reduced surface area for heat dissipation under the same current density.

3.4 Effect of thermal conductivity k_f

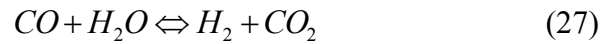
It is common that SOFC is fed with gas mixture instead of pure hydrogen. Moreover, water steam is produced in the electrochemical reaction process. Therefore, the gas composition and thermal conductivity of gas mixture (k_f) are usually different at different locations and under various operating conditions.

In the present study, the effect of k_f on ΔT_{sf} is examined in the range of 0.05~0.5W/(m K) (thermal conductivities of majority gas emerged in SOFC between 800~1200K are within this range) and is shown in Fig.6. As can be seen that ΔT_{sf} decreases with increasing k_f . This finding implies that ΔT_{sf} should increase with decreasing hydrogen molar fraction, as

hydrogen has a relatively larger thermal conductivity than other gases.

3.5 Direct internal reforming and ammonia thermal cracking reactions

For SOFCs running on hydrocarbon fuels, MSRR (Eq. 26) and WGSR (Eq. 27) are usually required. Compared with external reforming, direct internal reforming could simplify system as well as save energy[12], thus is commonly used in SOFC for hydrogen production.



For NH₃ fuel, ammonia thermal cracking reaction (ACR) can occur in SOFCs.



When CH₄ or NH₃ is used as fuel, Q to be dissipated through convection is reduced because both MSRR and WGSR are endothermic processes, and thus tends to reduce ΔT_{sf} (as shown in Fig.7). It can be seen that the magnitude of ΔT_{sf} increases sharply when operation temperature increases, especially for ammonia fed SOFC. The large temperature difference in NH₃ fueled SOFC is caused by very high reaction rates of ammonia thermal cracking at high temperatures [9]. For comparison, the reaction heat from MSSR is much smaller, due to relatively low reaction rates [12]. Even though, the value of ΔT_{sf} for NH₃ fueled SOFC is still about 1K. Therefore, from the present study, it can be seen that even including the internal reforming or ammonia thermal cracking reaction, the LTNE effect in SOFC electrode is still insignificant and the LTE assumption can be safely adopted for SOFC modeling in steady-state operation. It should be mentioned that in the start-up/shut-down cycles, the gas flow may be used for heating up or cooling down the cell, thus the temperature difference between

the gas and the solid could be larger. However, this temperature difference is not caused by the heat source terms and out of the scope of the present study. To examine the temperature difference in the heating up/cooling down process, detailed thermal-electrochemical modeling at the cell level is needed.

4. Conclusion

In this paper, the LTNE effect in SOFC electrode is studied under a wide range of operating/structural parameters. Different from the previous studies in the literature, half-reaction is used in the calculation for heat generation/consumption in the electrode. More importantly, both methane steam reforming reaction and ammonia thermal cracking reactions are considered. The temperature difference between solid and fluid phase (ΔT_{sf}) is used as an indicator of LTNE. Heat generation in different sources is calculated separately and TPB zone is regarded as the convective heat transfer area to examine the upper limit of ΔT_{sf} . Based on the framework proposed by Damm and Fedorov, a relationship is established for ΔT_{sf} prediction. It is found that ΔT_{sf} remains on the order of 10^{-3} K under a wide range of operating conditions and structural parameters for H_2 fueled SOFCs. It's also found that inclusion of MSRR and ACR changes ΔT_{sf} into more negative values. Particularly, the absolute value of ΔT_{sf} is the highest for NH_3 -fueled SOFC at high temperature (i.e. 1200K). But its value is still only about 1K, indicating insignificant LTNE effect in SOFC electrodes. In general, the LTE assumption can be safely adopted for thermal modeling of SOFCs running on hydrogen or alternative fuels, i.e. hydrocarbon fuels and ammonia.

Acknowledgement:

This research was supported by a grant (Project Number: PolyU 5238/11E) from Research Grant Council (RGC) of Hong Kong.

Symbols used

a_s	[$m^{-2}m^{-3}$]	specific heat transfer area
d	[μm]	solid particle diameter
F	[96485Cmol ⁻¹]	Faraday constant
h_{sf}	[$Wm^{-2}K^{-1}$]	heat transfer coefficient between gas and solid phases
i	[Am ⁻²]	current density
k_f	[$Wm^{-1}K^{-1}$]	thermal conductivity of fluid
L	[m]	thickness of electrolyte
L_{TPB}	[m.m ⁻³]	TPB length per unit volume
P	[atm]	partial pressure of gas species
Q	[Wm^{-3}]	heat generation/consumption rate
r_{ACR}	[molm ⁻³ s ⁻¹]	reaction rates of ACR
r_{MSRR}	[molm ⁻³ s ⁻¹]	reaction rates of MSRR
R	[8.3145Jmol ⁻¹ K ⁻¹]	universal gas constant
w	[m]	effective width of TPB region
ΔH_{ACR}	[Jmol ⁻¹]	enthalpy change of ACR
ΔH_{MSRR}	[Jmol ⁻¹]	enthalpy change of MSRR
ΔS	[Jmol ⁻¹ K ⁻¹]	entropy change
ΔT_{sf}	[K]	temperature difference between the solid and the gas phases
θ_p	[-]	porosity of electrode

References

- [1] A. Sciacovelli, V. Verda, *Energy* **2009**, 34 (7): 850-865.
- [2] J.J. Hwang, P.Y. Chen, *Int.J. Heat Mass Transfer* **2006**, 49 (13–14): 2315-2327.
- [3] D.L. Damm, A.G. Fedorov, *J. Power Sources* **2006**, 159 (2): 1153-1157.
- [4] F. Kuwahara, M. Shirota, A. Nakayama, *Int. J. Heat Mass Transfer* **2001**, 44 (6): 1153-1159.
- [5] A.M. Gokhale, S. Zhang, M. Liu, *J. Power Sources* **2009**, 194 (1): 303-312.
- [6] A. Hafsia, Z. Bariza, H. Djamel, B.M. Hocine, G.M. Andreadis, A. Soumia, *Energy Procedia* **2011**, 6: 643-650.
- [7] K. Fischer, J.R. Seume, *J. Fuel Cell Sci. Technol.* **2009**, 6 (1): 011002-011011 .
- [8] S.K. Ratkje, Y. Tomii, *J. Electrochem. Soc.* **1993**, 140 (1): 59-66.
- [9] B.A. Haberman, J.B. Young, *Int. J. Heat Mass Transfer* **2004**, 47 (17–18): 3617-3629.
- [10] M. Ni, M.K.H. Leung, D.Y.C. Leung, *Int. J. Energy Res.* **2009**, 33 (11): 943-959.
- [11] W. Sangtongkitcharoen, S. Assabumrungrat, V. Pavarajarn, N. Laosiripojana, P. Praserttham, *J. Power Sources* **2005**, 142 (1–2): 75-80 .
- [12] M. Ni, *J. Power Sources* **2011**, 196 (4): 2027-2036.
- [13] J. Fleig, A. Schintlmeister, A.K. Opitz, H. Hutter, *Scr. Mater.* **2011**, 65 (2): 78-83.
- [14] F.H. van Heuveln, H.J.M. Bouwmeester, F.P.F. van Berkel, *J. Electrochem. Soc.* **1997**, 144 (1): 126-133.
- [15] T. Horita, K. Yamaji, N. Sakai, Y. Xiong, T. Kato, H. Yokokawa, T. Kawada, *J. Power Sources* **2002**, 106 (1–2): 224-230.
- [16] Y. Yan, S.C. Sandu, J. Conde, P. Muralt, *J. Power Sources* **2012**, 206: 84-90.
- [17] M. Andersson, J. Yuan, B. Sunden, *Int. J. Heat Mass Transfer* **2012**, 55 (4): 773-788.
- [18] M. Ni, M.K.H. Leung, D.Y.C. Leung, *J. Power Sources* **2007**, 168(2): 369-378.

List of Figures

Figure 1 Schematic diagram of local structure in porous electrode

Figure 2. Effects of operating temperature and particle size on ΔT_{sf}

Figure 3. Effect of porosity θ_p on ΔT_{sf}

Figure 4. Effect of TPB width w on ΔT_{sf}

Figure 5. Effect of reaction depth L on ΔT_{sf}

Figure 6. Effect of thermal conductivity on ΔT_{sf}

Figure 7. Effect of internal reforming reactions on ΔT_{sf}

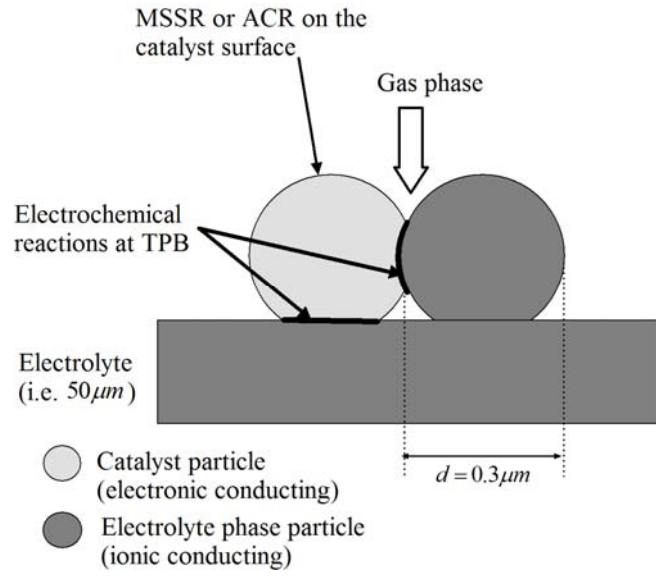


Figure 1

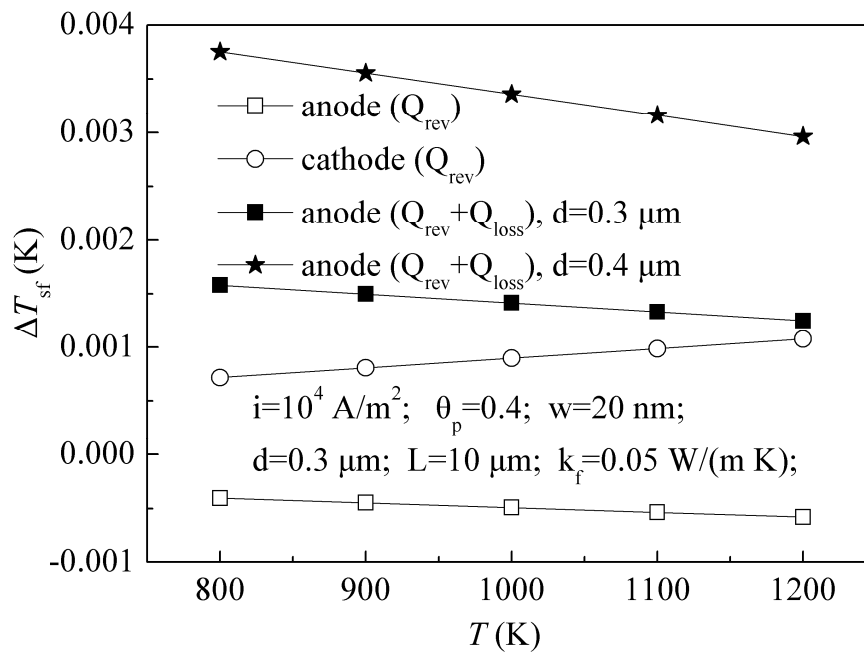


Figure 2

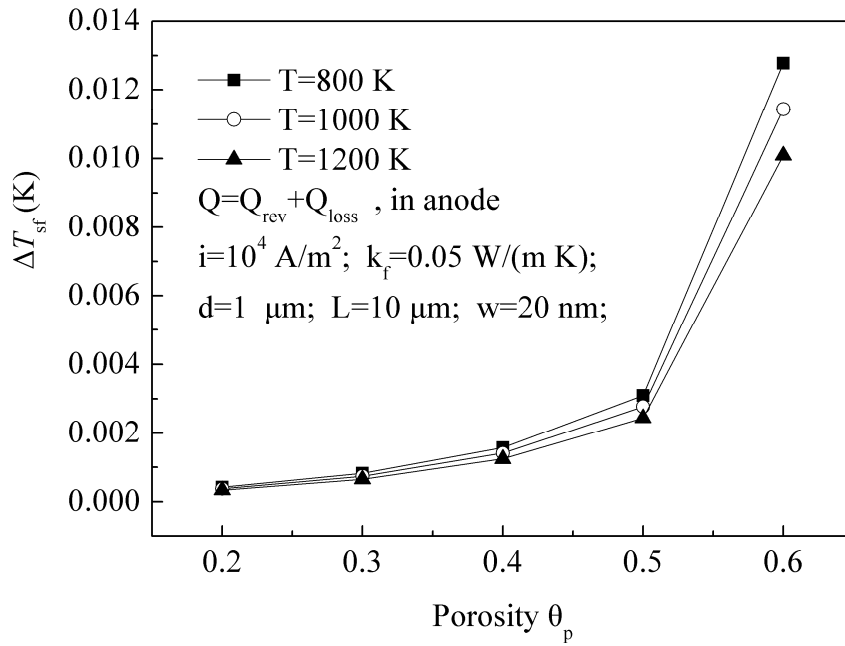


Figure 3

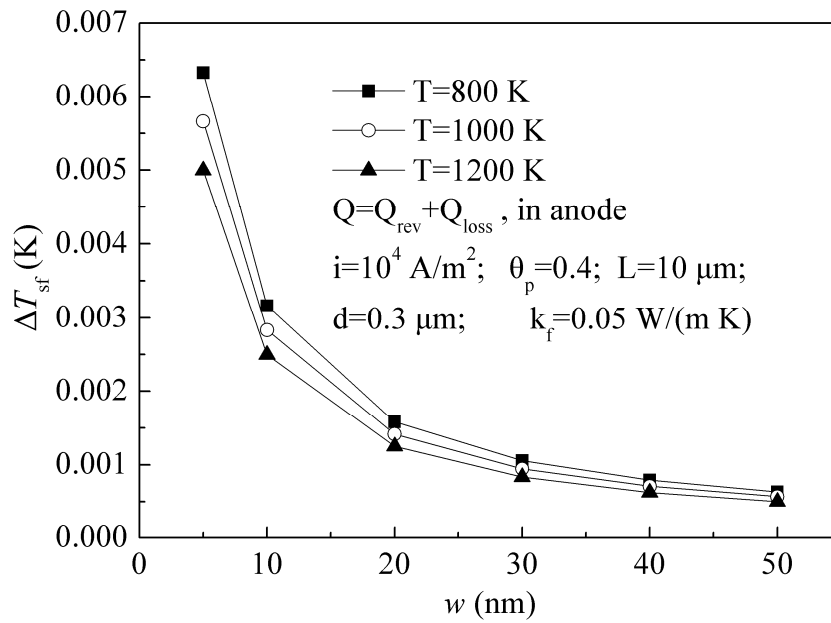


Figure 4

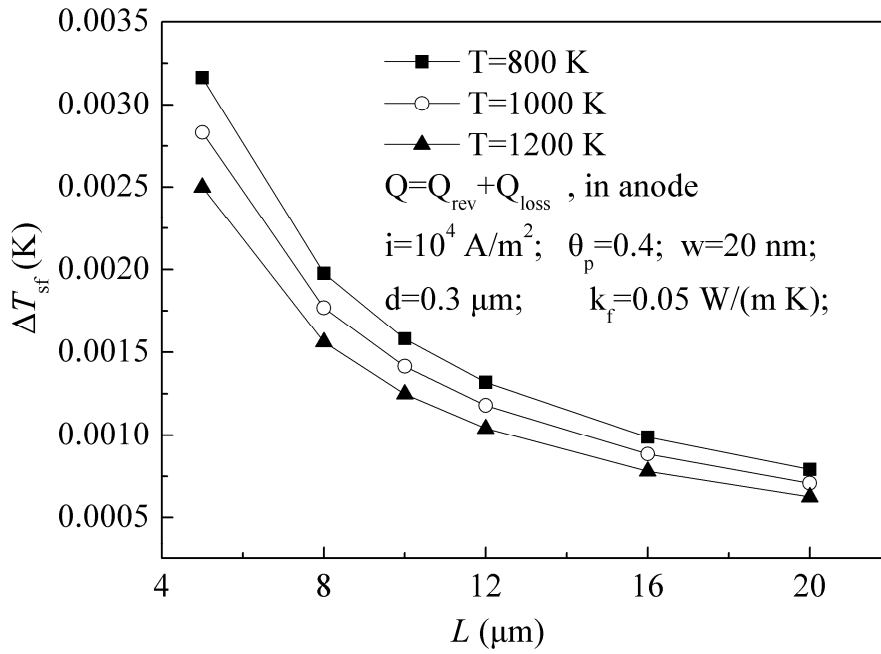


Figure 5

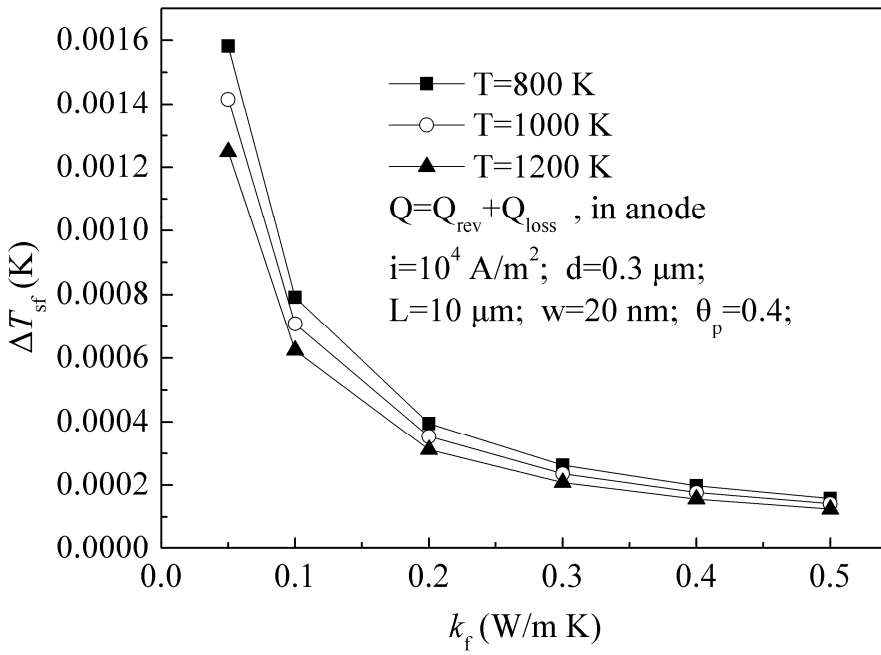


Figure 6

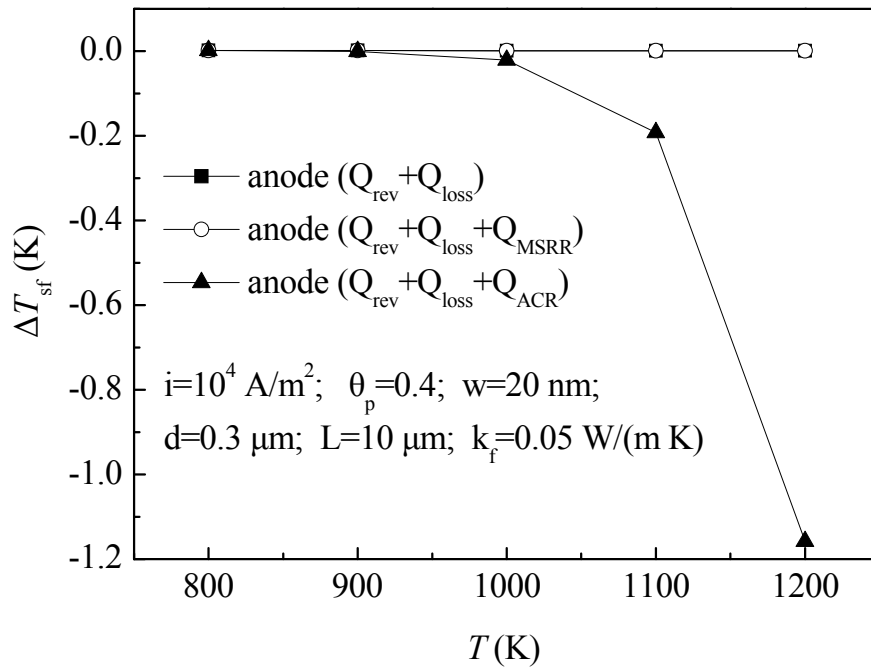


Figure 7